


## Imprinting spiral Higgs waves onto superconductors with vortex beams

Takeshi Mizushima<sup>1,\*</sup> and Masahiro Sato<sup>2,†</sup>

<sup>1</sup>*Department of Materials Engineering Science, Osaka University, Toyonaka, Osaka 560-8531, Japan*

<sup>2</sup>*Department of Physics, Chiba University, Chiba 263-8522, Japan*

 (Received 18 June 2023; revised 19 September 2023; accepted 20 September 2023; published 4 October 2023)

A vortex beam, akin to a quantized vortex in superfluids, possesses inherent orbital angular momentum (OAM), resulting in the propagation of a spiral-shaped wavefront. Here, we demonstrate that a pulsed vortex beam with OAM in the terahertz frequency band can induce a spiral Higgs wave, which is a spiral-shaped oscillation mode of the superconducting order parameter. By utilizing the gauge-invariant theory for the superconducting order, we demonstrate that the phase mode is driven to screen the longitudinal magnetic field of the vortex beam, which facilitates the imprinting of the spiral-shaped wavefront and the transfer of OAM to the condensate. Furthermore, we find that increasing the OAM of light amplifies the intensity of the third-harmonic generation. These findings highlight the potential of terahertz vortex beams as a spectroscopic probe of collective modes.

DOI: [10.1103/PhysRevResearch.5.L042004](https://doi.org/10.1103/PhysRevResearch.5.L042004)

**Introduction.** In 1992, Allen *et al.* [1] discovered the vortex beam, a light beam with a spiral-shaped wavefront around its propagation axis. Similar to a quantum vortex in superfluids, a vortex beam has a phase singularity and carries both orbital angular momentum (OAM) of  $m\hbar$  and spin angular momentum (SAM). SAM designates the handedness of light, while the topological charge of OAM,  $m \in \mathbb{Z}$ , counts the number of phase windings in a single wavelength. The phase singularity gives rise to a doughnut-shaped intensity distribution [1–3]. Vortex beams have been developed as essential optical techniques for a wide range of optical and physical phenomena, including optical trapping and manipulation [4–9], quantum communications [10–12], chiral nanostructure fabrication [13–15], optical vortex knots [16], and astrophysics [17]. Although the research field of vortex beams is continuously expanding, the applications for solid-state physics are still limited.

The recent development of generating vortex beams with high intensity in the terahertz (THz) band has exciting implications for solid-state physics [18–24]. THz vortex beams offer a unique opportunity for ultrafast manipulation of states of matter since photon energy is comparable to that of collective excitations in materials, such as spin waves. The coupling between THz vortex beams and ordered spin structure in magnets leads to the OAM dichroic effect [20,22] and Faraday effect [24]. Furthermore, the imprint of the helical structure of vortex beams on spin texture has been demonstrated in a

semiconductor quantum well [23]. Theoretical studies have also revealed that vortex beams cause nonequilibrium phenomena in magnets, including the generation of spiral spin waves and topological defects [25,26].

In this Letter, we theoretically study the nonlinear optical responses of superconductors to THz vortex beams. These beams align with the distinctive length scale of superconductors, such as long-wavelength spin waves and topological defects in magnets [25,26]. Given that the coherence length of Cooper pairs is extensive, the macroscopic wave function can effectively capture characteristic wavefronts of vortex beams. The THz band is necessary since its photon energy is compatible with the Higgs mode. Throughout numerical simulations on the effective action of the superconducting order and gauge fields, we demonstrate that pulsed vortex beams significantly enhance the intensity of third-harmonic generation (THG) by driving the spiral-shaped Higgs waves in the condensate. This occurs due to the quadratic coupling of the amplitude oscillation to gauge-invariant potentials. The spacetime phase (plasma) fluctuations are responsible for imprinting the spiral-shaped wavefronts to the condensate and amplifying the THG intensity with the OAM of light. These findings suggest that THz vortex beams serve as spectroscopic probes for collective modes.

**Laguerre-Gaussian vortex beam.** Vortex beams are a class of solutions of Maxwell's equations within the paraxial approximation that carries OAM [1,27]. They are often referred to as Laguerre-Gaussian modes. When considering a monochromatic incident electric field and propagation in the  $z$  direction, the field configuration can be expressed as  $\mathbf{E}^{\text{ext}}(\mathbf{x}, t) = i\Omega[\hat{\epsilon}_s u_{p,m} + \hat{\mathbf{z}}_k^i (\hat{\epsilon}_s \cdot \nabla) u_{p,m}] e^{-i\Omega t}$ , where  $\hat{\epsilon}_s = (\hat{\mathbf{x}} + is\hat{\mathbf{y}})/\sqrt{2}$  is the polarization vector for circularly polarized light and  $s = \pm 1$  is the SAM of light. Let  $\mathbf{x} = (\rho, \theta, z)$  be the cylindrical coordinate, where  $\rho = \sqrt{x^2 + y^2}$  and  $\theta = \arctan(y/x)$ . The spatial profile of  $u_{p,m}$  at the focal plane

\*mizushima@mp.es.osaka-u.ac.jp

†sato.phys@chiba-u.jp

Published by the American Physical Society under the terms of the [Creative Commons Attribution 4.0 International license](https://creativecommons.org/licenses/by/4.0/). Further distribution of this work must maintain attribution to the author(s) and the published article's title, journal citation, and DOI.

( $z = 0$ ) is given by

$$u_{p,m}(\rho, \theta, z = 0) = \left(\frac{\rho}{w_0}\right)^{|m|} e^{-\rho^2/w_0^2} e^{im\theta} L_p^{|m|}\left(\frac{2\rho^2}{w_0^2}\right), \quad (1)$$

where  $L_p^{|m|}$  is the associated Laguerre polynomial and  $w_0$  is the diameter of the Gaussian beam. Apart from  $s = \pm 1$ , the Laguerre-Gaussian mode is identified by  $p, m \in \mathbb{Z}$ . The integer  $p$  corresponds to the number of nodes for the radial direction, while  $m$  represents the topological charge associated with the OAM of light. This delineates the phase accumulated in multiples of  $2\pi$  when traveling around the mode circumference. The winding number of the spiral-shaped wavefront can determine the helicity or handedness of the wavefront. Vortex beams with  $m \neq 0$  have a ‘‘doughnut-shaped’’ intensity profile, with peak intensity around  $\rho \sim w_0$ . Gaussian beams, corresponding to  $m = 0$ , have been employed in the spectroscopy of the Higgs excitations [28–38]. Unlike conventional Gaussian beams, the vortex beam involves a longitudinal component of the magnetic field,  $\mathbf{B}_z^{\text{ext}} = (\nabla \times \mathbf{A}^{\text{ext}})_z \propto \cos(J\theta - \Omega t)$ . Below we show that in superconductors, the phase mode screens the longitudinal field, which is essential for imprinting the spiral wavefront of light to the condensate.

*Nonlinear dynamics induced by vortex beams.* To study the nonlinear dynamics of superconductors induced by vortex beams, we start with the effective action at  $T = 0$  [39–41],

$$\mathcal{S} = \int dx \left[ -\tau |\mathcal{D}_t \Delta(x)|^2 - \gamma \Delta^*(x) \mathcal{D}_t \Delta(x) + \kappa |\mathcal{D} \Delta(x)|^2 + \alpha |\Delta(x)|^2 + \frac{\beta}{2} |\Delta(x)|^4 + \frac{\mathbf{B}^2(x) - \mathbf{E}^2(x)}{8\pi} \right], \quad (2)$$

where  $\Delta(x)$  is the superconducting order parameter. Here, we introduce  $x \equiv (\mathbf{x}, t)$ , and  $(\tau, \kappa, \alpha)$  are microscopically determined [42]. The wave speed and coherence length are defined as  $v^2 \equiv \kappa/\tau = v_F^2/3$  and  $\xi_0^2 \equiv \kappa/|\alpha| = v^2/2\Delta_0^2$ , respectively, where  $\Delta_0$  is the superconducting gap at equilibrium and  $v_F$  is the Fermi velocity of normal electrons. These values characterize the wave propagation and length scale of  $\Delta(x)$ . The scalar and vector potentials  $(\Phi, \mathbf{A})$  are coupled to  $\Delta$  through covariant derivatives  $\mathcal{D}_t \equiv \partial_t + 2ie\Phi$  and  $\mathcal{D} \equiv \nabla - i\frac{2e}{c}\mathbf{A}$ . The internal electromagnetic (EM) fields in the superconductor are defined as  $\mathbf{B} = \nabla \times \mathbf{A}$  and  $\mathbf{E} = -\nabla\phi - \frac{1}{c}\partial_t\mathbf{A}$ , where  $\phi \equiv \Phi - \phi^{\text{ext}}$  and  $\mathbf{A} \equiv \mathbf{A} - \mathbf{A}^{\text{ext}}$  are the scalar and vector potentials in the superconductor, respectively, and the external potentials generated by vortex beams are represented by  $\phi^{\text{ext}} = 0$  and  $\mathbf{A}^{\text{ext}} = \mathbf{E}^{\text{ext}}/i\Omega$ . In this Letter, we set  $\hbar = 1$ . The first term in Eq. (2) pertains to collective excitations, while the second term, which involves  $\gamma$ , contributes to the dissipation of these modes back to equilibrium. When the energy scale of the excitations satisfies  $\omega \lesssim 2\Delta_0$ , the damping is suppressed because of the absence of the fermionic excitations. Therefore, we determine  $\gamma$  to satisfy  $\gamma \ll \tau\omega$ .

The equation of motion (EOM) for  $\Delta$ , derived from Eq. (2), has a wavelike form with a relaxation term [42]. The gauge fields are governed by Ampère’s law and Gauss’s law,

$$\nabla \times \mathbf{B}(x) - \frac{1}{c} \partial_t \mathbf{E}(x) = \frac{4\pi}{c} \mathbf{j}(x), \quad \nabla \cdot \mathbf{E}(x) = 4\pi \rho(x), \quad (3)$$

where the charge and supercurrent densities are  $\rho(x) = 2ie\tau \Delta^*(x) \mathcal{D}_t \Delta(x) + \text{c.c.}$  and  $\mathbf{j}_\mu(x) = -2eik \Delta^*(x) \mathcal{D}_\mu \Delta(x) + \text{c.c.}$ , respectively. We introduce the dissipation of the EM fields by replacing  $\mathbf{j}$  with  $\mathbf{j}_{\text{tot}} = \mathbf{j} + \mathbf{j}_n$ . Here,  $\mathbf{j}_n = \sigma_n \mathbf{E}$  is the dissipative current that follows the Ohmic law. The EOMs obey the charge conservation law,  $\partial_t \rho + \nabla \cdot \mathbf{j} = 0$ .

Equation (2) is the nonrelativistic U(1) Higgs model, which describes the collective modes in bulk superconductors [40]. Let us consider small amplitude and phase fluctuations of the condensate around  $\Delta_0$ ,  $\Delta(x) = [\Delta_0 + \delta\Delta(x)]e^{i\varphi(x)}$ . For  $|\Delta(x)| = \Delta_0$ , the U(1) phase  $[\varphi(x)]$  is absorbed into the gauge fields through the gauge transformation. As a result, the longitudinal component of the gauge field gains a mass gap of  $\omega_p = \sqrt{4\pi e^2 n/m_e}$ , where  $n$  is the electron density and  $m_e$  is the mass of electrons. Then, the only low-lying collective excitation is the Higgs mode with the dispersion  $\omega_H^2(\mathbf{q}) = 4\Delta_0^2 + v^2 q^2$ . The action has been utilized for the numerical simulations of spontaneous vortex formation [43] and collisional dynamics of vortices [44]. For numerical calculations, we take the temporal gauge that  $\phi = 0$  in all time [44–47], and implement methods from the Hamiltonian formalism of the lattice gauge theory to ensure gauge invariance and charge conservation [42,44,48].

We first consider a superconducting film with a thickness ( $d$ ) that is less than the London penetration depth  $\lambda$  and  $\xi_0$ . Then, the dynamics of  $\Delta(x)$  and  $\mathbf{j}(x)$  can be restricted to two dimensions. Starting at the equilibrium state,  $\Delta(\mathbf{x}, t = 0) = \Delta_0$ , we irradiate a pulsed vortex beam for  $t > 0$  [Fig. 1(a)]. Since the wavelength of THz vortex beams is significantly longer than both  $d$  and  $\lambda$ , we can disregard the  $z$  dependence of  $\mathbf{A}^{\text{ext}}$ . The vector potential for the pulsed vortex beam with  $(m, s)$  is given by

$$\mathbf{A}^{\text{ext}}(\mathbf{x}, t) = \text{Re} \left\{ \frac{A_0 u_{p,m}(\mathbf{x})}{\max |u_{p,m}(\mathbf{x})|} \exp \left[ -\left(\frac{t-t_0}{\sigma}\right)^2 - i\Omega t \right] \hat{e}_s \right\}, \quad (4)$$

where  $\Omega$  and  $\sigma \equiv 2\pi n_p/\Omega$  are the frequency and the full width at half maximum of the beam intensity, respectively. In this work, we consider vortex beams with  $p = 0$ . In the following calculations, we take the number of cycles of the pulse field and the beam waist as  $n_p = 5$  and  $w_0 = 20\xi_0$ , respectively. We also set  $t_0 = 2\sigma$  and the size of the  $xy$  plane to  $x, y \in [-200\xi_0, 200\xi_0]$ . In the Supplemental Material [42], we clarify that  $n_p$  and  $w_0$  do not alter the dynamics of  $\Delta(x)$  and EM waves. In conventional superconductors,  $\xi_0$  and  $\lambda$  are  $O(10\text{--}100 \text{ nm})$ . For instance, bulk Nb has  $\xi_0 \sim \lambda \sim 40 \text{ nm}$  [49] and NbN thin films have a large value of the Ginzburg-Landau (GL) parameter  $\kappa_{\text{GL}} \equiv \lambda/\xi_0$  with  $\xi_0 \sim 5 \text{ nm}$  and  $\lambda \sim 200 \text{ nm}$  [50]. The timescale is represented by  $t_\Delta \equiv \hbar/\Delta_0 = O(1 \text{ ps})$  with  $\Delta_0 = O(1 \text{ meV})$ . In the following calculations, the coefficient in Eq. (4) is fixed to  $2|e|\xi_0 A_0/\hbar c = 0.4$ , corresponding to the maximum electric field of  $E_0 \equiv \Omega A_0 = 0.4 \text{ kV/cm}$  with  $\xi_0 = 10 \text{ nm}$  and  $\Omega = 0.5 \text{ THz}$ . In the current work, the heating effect is not taken into account since laser absorption has a minimal impact on THz vortex beams. For ultraviolet-visible vortex beams, however, the heating effect becomes more substantial [26,51,52].

Figure 1(b) shows the spatial profile of the internal magnetic field  $B_z(\mathbf{x}, t)$  and the supercurrent density  $\mathbf{j}(\mathbf{x}, t)$

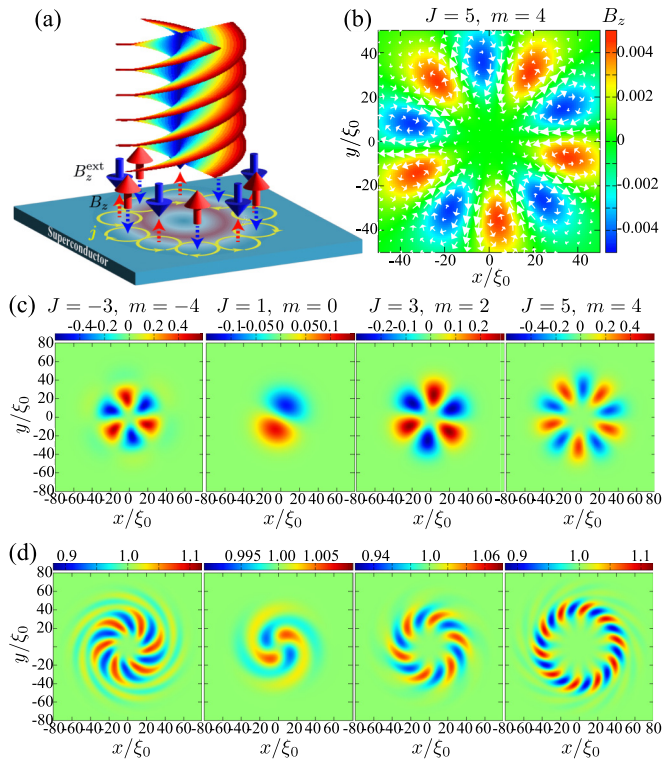


FIG. 1. (a) Schematics of our setup, where the spiral shape depicts the wavefront of the vortex beam with  $m = 4$ . The vortex beam with  $m \neq 0$  involves  $B_z^{\text{ext}}$ , which is screened by the internal field  $B_z$  and the supercurrent density  $\mathbf{j}$ . (b) Spatial profiles of  $B_z(\mathbf{x}, t)$  (color map) and  $\mathbf{j}(\mathbf{x}, t)$  (arrows) at  $t = 51t_\Delta$ , driven by the vortex beam with  $(m, s) = (4, 1)$ . (c), (d) Snapshots of (c) the charge density  $\rho(\mathbf{x}, t)$  at  $t = 51t_\Delta$  and (d) the condensate amplitude  $|\Delta(\mathbf{x}, t)|$  at  $t = 153t_\Delta$ , induced by vortex beams with  $J = m + s$ , where  $t_\Delta \equiv \hbar/\Delta_0 = O(1 \text{ ps})$  represents the timescale of the condensate. The intensity of the pulsed vortex beam almost becomes maximum around  $t = 62t_\Delta$ . In all data, we set  $\Omega = 1.025\Delta_0$ , close to the nonlinear Higgs resonance.

(arrows) at  $t = 51t_\Delta \sim t_0$ , driven by the circularly polarized vortex beam with  $(m, s) = (4, 1)$ . Here, we set the GL parameter to be close to the nonlinear resonance of the Higgs mode,  $\Omega = 1.025\Delta_0$ . The induced supercurrent generates the internal field  $B_z(\mathbf{x}, t) \propto -B_z^{\text{ext}}(\mathbf{x}, t)$ , which screens the external field  $B_z^{\text{ext}}(\mathbf{x}, t)$ . The charge conservation dictates that the inhomogeneous current density in the plane is accompanied by a fluctuation in the charge density as  $\partial_t \rho = -\nabla \cdot \mathbf{j}$ . In Fig. 1(c), we present the snapshots of  $\rho(\mathbf{x}, t)$  at  $t = 51t_\Delta$  for  $m = -4, 0, 2$ , and  $4$  ( $J = -3, 1, 3$ , and  $5$ ), which yield the oscillation pattern that reflects the total angular momentum of light  $J$ . In Fig. 1(d), we observe that the oscillation pattern of the condensate amplitude along the azimuthal direction carries twice the total angular momentum  $2J$ .

Figure 2 shows how vortex beams induce the dynamics of the condensate and charge density. Here, we focus on  $(m, s) = (4, 1)$  and  $\Omega = 1.025\Delta_0$ . In Fig. 2(a), we display the snapshots of  $|\Delta(\mathbf{x}, t)|$  and  $\rho(\mathbf{x}, t)$  after irradiating the pulsed wave in Eq. (4) onto the condensate. For  $t \lesssim t_0/2 = 10\pi t_\Delta$ , the vortex beam mainly stimulates the charge density with the

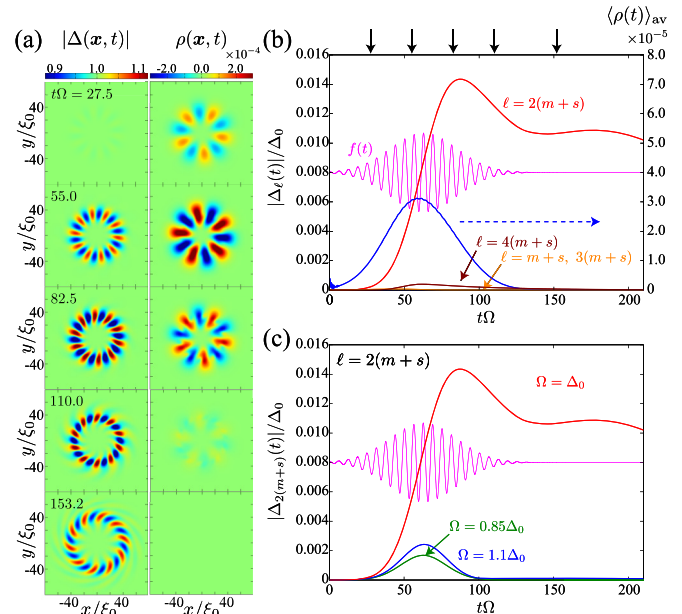


FIG. 2. (a) Snapshots of  $|\Delta(\mathbf{x}, t)|$  and  $\rho(\mathbf{x}, t)$  at  $t\Omega = 27.5, 55.0, 82.5, 110.0$ , and  $137.5$  for  $\Omega = 1.025\Delta_0$  and  $(m, s) = (4, 1)$ , where  $\Omega^{-1} = 0.6 \text{ ps}$  for  $\Delta_0 = 1 \text{ meV}$ . (b) Time evolutions of the projections of  $\Delta$  onto angular momentum eigenstates ( $\Delta_\ell$ ) with  $\ell = J, 2J, 3J$ , and  $4J$ . The amplitudes of the other  $\ell$  components are negligibly small. In (a), we also plot the spatially averaged charge density fluctuation  $\langle |\rho(t)| \rangle_{\text{av}}$ . (c) Time evolutions of  $\Delta_{\ell=2J}$  for  $\Omega/\Delta_0 = 0.85, 1.0$ , and  $1.1$ . In (b) and (c), the magenta curve shows the temporal profile of the applied field  $f(t) = \cos(\Omega t)e^{-(t-t_0)^2/\sigma^2}$ .

peak intensity around  $t \sim t_0$ . Subsequently, a spiral-shaped wave appears on the condensate  $\Delta(\mathbf{x})$ , persisting even after the charge density fluctuation  $\rho(\mathbf{x})$  is fully screened. We expand the condensate wave function in terms of the eigenstates of the angular momentum as  $\Delta(\theta, t) \equiv \int \Delta(\mathbf{x}, t) d\rho = \sum_\ell e^{i\ell\theta} \Delta_\ell(t)$  ( $\ell \in \mathbb{Z}$ ). In Fig. 2(b), we find that  $\Delta_\ell$  with  $\ell = 2J$  significantly increases around  $t \sim t_0$ , while the other components with  $\ell \neq 2J$  are almost negligible. The time evolution of the net charge density excitation,  $\langle \rho(t) \rangle_{\text{av}} \equiv \int d\mathbf{x} |\rho(\mathbf{x}, t)|$ , is also shown in Fig. 2(b). This excitation follows the envelope of the pulsed field  $e^{-(t-t_0)^2/\sigma^2}$ . The charge density is excited before the oscillation of the condensate amplitude grows, and it returns to neutral once the pulse is off. As mentioned below, the charge density oscillation is associated with the off-resonant phase excitation and only transiently excited. In Fig. 2(c), we observe a sharp reduction in the intensity of  $\Delta_{2J}(t)$  as the frequency  $\Omega$  deviates from the nonlinear resonance to the Higgs mode,  $\Omega = \Delta_0$ .

*Gauge-invariant response and enhancement of THG.* Let us now examine the results in Figs. 1 and 2, based on the analysis of the effective action. The phase of the superconducting order  $\varphi$ , defined by  $\Delta = |(\Delta_0 + \delta\Delta)|e^{i\varphi}$ , is essential for the gauge invariance of the theory. Here, we clarify that vortex beams carrying nonzero OAM stimulate phase excitations, which strengthen the gauge-invariant quadratic coupling of the vortex beams to the Higgs mode ( $\delta\Delta$ ) and amplifies the nonlinear current responses.

To uncover the role of the phase fluctuation, let us focus on the gauge-invariant potential  $\tilde{\mathcal{A}}(\mathbf{x}) \equiv \mathcal{A}(\mathbf{x}) - \frac{c}{2e} \nabla\varphi(\mathbf{x})$ .

Solving the continuity equation and the Maxwell-Ampère law in the linear response regime, the potential reads [42]

$$\tilde{\mathcal{A}}(x) \approx -\frac{(\kappa_{\text{GL}}/C)^2}{1 - (\kappa_{\text{GL}}/C)^2} A_{\perp}^{\text{ext}}(x) - \frac{ic}{2e} \frac{\nabla[\nabla \cdot A_{\perp}^{\text{ext}}(x)]}{(\omega_{\text{p}}/v)^2}, \quad (5)$$

for  $\Omega \sim \Delta_0$ , where  $C \sim c/v$  and  $A_{\perp}^{\text{ext}} = (A_x^{\text{ext}}, A_y^{\text{ext}}, 0)$ . The first term pertains to the screening effect, while the second term is attributed to the off-resonant phase excitation  $\nabla\varphi$ . In the low  $\kappa_{\text{GL}}$  regime, the internal field is induced to screen  $A_{\perp}^{\text{ext}}$  and the first term vanishes at the type-I limit,  $\kappa_{\text{GL}} \rightarrow 0$ . As a result,  $B_z^{\text{ext}}$  generated by vortex beams is screened by the internal field  $B_z$ , while the transverse fields ( $B_x^{\text{ext}}, B_y^{\text{ext}}$ ) remain unscreened in a thin film. On the other hand, at the type-II limit ( $\kappa_{\text{GL}} \rightarrow \infty$ ), the screening current is negligible, and the first term of Eq. (5) reduces to  $A_{\perp}^{\text{ext}}$ . The second term represents the off-resonant phase excitation, where the THz range is far from the resonance  $\Omega \ll \sqrt{(vq)^2 + \omega_{\text{p}}^2} \approx \omega_{\text{p}}$ . The phase excitation is linearly driven by vortex beams as  $\varphi(x) \propto \nabla \cdot A_{\perp}^{\text{ext}}(x) \propto \hat{e}_s \cdot \nabla e^{im\theta - i\Omega t} u_{p,m}(x)$ , indicating that the oscillation pattern of the phase mode reflects the OAM of light as  $\varphi(x) \propto m \cos(J\theta - \Omega t)$ . This explains the characteristic oscillation pattern of  $\rho(x, t) \propto \partial_t \varphi(x, t) \propto m \cos(J\theta - \Omega t)$  shown in Fig. 1(c). Thus the OAM of light can be encoded to the superconductor in the form of the charge density oscillation. It is also worth mentioning that the intensity of the first term in Eq. (5) is insensitive to the OAM of light,  $m$ , while the second term is proportional to  $m$ . In the low  $\kappa_{\text{GL}}$  regime, the first term in Eq. (5) is screened, while the impact of the second term becomes prominent. Then, the intensity of the gauge-invariant potential ( $\tilde{\mathcal{A}}$ ) amplifies through the off-resonant phase excitation as  $m$  increases. This is a unique feature of vortex beams and absent in conventional Gaussian beams with  $m = 0$ .

The phase excitation and the screening effect affect the coupling of light to the Higgs mode the THG intensity. From Eq. (2), the third-order current response is given as

$$\mathbf{j}^{(3)}(x, t) = -\frac{16e^2\kappa\Delta_0}{c} \delta\Delta(x, t) \tilde{\mathcal{A}}(x, t), \quad (6)$$

which is mediated by the Higgs excitations ( $\delta\Delta$ ). The Higgs mode ( $\delta\Delta$ ) is coupled to  $\tilde{\mathcal{A}}$  through the effective action

$$S_{\delta\Delta A} \equiv \frac{4e^2\kappa}{c^2} \int dx |\delta\Delta(x)|^2 \tilde{\mathcal{A}}^2(x). \quad (7)$$

As mentioned above, the potential is approximated as  $\tilde{\mathcal{A}} \sim -\frac{2e}{c} \nabla\varphi$  in the low  $\kappa_{\text{GL}}$  regime, and its quadratic form involves  $\varphi^2 \propto (\hat{e}_s \cdot \nabla e^{im\theta - i\Omega t})^2 \propto \sin^2(J\theta - \Omega t)$ , which generates the spiral wave in the condensate with a period of  $2\pi w_0/2J$ . For Gaussian beams with  $m = 0$ , only the direct coupling of  $\delta\Delta$  and  $(\tilde{\mathcal{A}})^2 \approx (A^{\text{ext}})^2$  in Fig. 3(a) is possible and the phase mode is not active. In the case of vortex beams with  $m \neq 0$ , however, the inhomogeneity causes the off-resonant phase excitations and enhances the gauge-invariant potential with increasing  $|m|$ . Figure 3(b) depicts the impact of the phase mode on  $\tilde{\mathcal{A}}$ , which strengthens both the nonlinear Higgs excitation and the nonlinear current response.

To verify the aforementioned scenario, we compute the THG intensity for different values of  $\Omega$ ,  $m$ , and  $\kappa_{\text{GL}}$ . The THG intensity is defined as  $I(3\Omega) =$

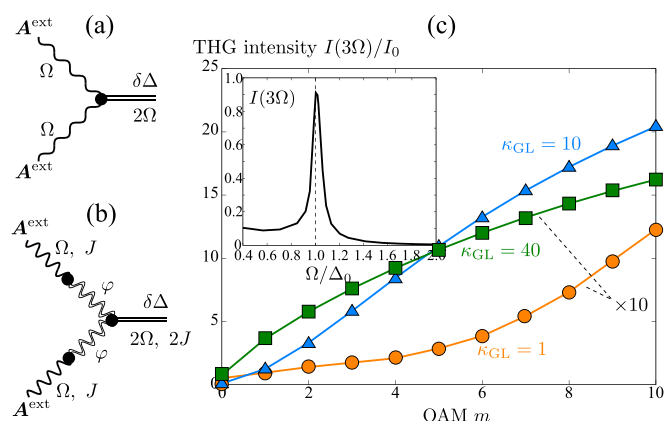


FIG. 3. (a), (b) Diagrams of nonlinear Higgs excitations by vortex beams: (a) The coupling to  $(A^{\text{ext}})^2$  and (b) the quadratic coupling through the phase modes. (c)  $m$  dependence of the THG intensity  $I(3\Omega)/I_0$  at  $\Omega = 1.025\Delta_0$  for  $\kappa_{\text{GL}} = 1$  (circles), 10 (triangles), and 40 (squares), where  $I_0 \equiv c^2/(16\pi e)$ . The inset shows the THG intensity  $I(3\Omega)$  for  $(m, s) = (4, 1)$  and  $\kappa_{\text{GL}} = 10$ .

$\int dt I(t) e^{i3\Omega t}$  with  $I(t) \equiv \int dx |\mathbf{j}(x, t)|$ . As shown in Eq. (6), the nonlinear Higgs excitation contributes to the THG as  $I(3\Omega) \propto \int dq \tilde{\mathcal{A}}(\mathbf{q}, \Omega) \tilde{\mathcal{A}}^2(-\mathbf{q}, -2\Omega) / \{(2\Omega)^2 - [\omega_{\text{H}}(\mathbf{q})]^2\}$ , and the gauge-invariant potential involves the off-resonant phase excitations. In Fig. 3(c), the inset displays the THG intensity  $I(3\Omega)$  for  $(m, s) = (4, 1)$ . The spectrum exhibits a distinct peak at the nonlinear Higgs resonance frequency  $\Omega = \Delta_0$ . The main panel of Fig. 3(c) indicates that the weak intensity of the THG at  $m = 0$  increases as  $|m|$  increases. This aligns with the scenario where a vortex beam with  $m \neq 0$  linearly drives a spacetime fluctuation of the phase mode, enhancing the nonlinear coupling of the Higgs mode to light through the gauge-invariant potential.

The THG intensity is influenced by  $\kappa_{\text{GL}}$ . As shown in Fig. 3(c), the THG intensity at  $\kappa_{\text{GL}} = 1$  is approximately ten times weaker than that at  $\kappa_{\text{GL}} = 10$  due to the strong screening effect, but it is significantly amplified by the OAM of light. The  $\kappa_{\text{GL}}$  dependencies are attributed to the interplay between the screening effect and off-resonant plasma oscillation. As mentioned in Eq. (5), the gauge-invariant potential  $\tilde{\mathcal{A}}$  consists of  $A^{\text{ext}}$  and the off-resonant phase excitation. In the low  $\kappa_{\text{GL}}$  regime ( $\kappa_{\text{GL}} = 1, 10$ ), the former is screened, and  $\tilde{\mathcal{A}}$  is dominated by the latter term which amplifies with  $m$ . For  $\kappa_{\text{GL}} \gg 1$ , however, the screening effect weakens and the potential reduces to  $\tilde{\mathcal{A}} \approx A^{\text{ext}}$ . The nonlinear current response in  $\kappa_{\text{GL}} = 40$  is governed by  $A^{\text{ext}}$  rather than off-resonant plasma excitations. As a result, the increase of the THG intensity with  $m$  is suppressed for  $\kappa_{\text{GL}} \gg 1$ . There are optimal values of  $\kappa_{\text{GL}}$  that maximize the THG intensity [42]. We also note that the result in Fig. 3(c) is insensitive to  $w_0$  [42].

*Spiral waves on the surface of SCs.* So far, we have focused on two dimensions. However, comparable outcomes can be seen even when we take into account a finite thickness along the  $z$  axis. Consider a superconducting film with a thickness of  $d = 20\xi_0$  and the penetration depth of  $\lambda = 10\xi_0$  ( $\kappa_{\text{GL}} = 10$ ). The vortex beam is irradiated towards the upper surface of the film at  $z = d/2$ . Figure 4 shows the snapshots of  $|\Delta(x, t)|$  [Fig. 4(a)],  $\rho(x, t)$  [Fig. 4(b)], and  $\mathbf{j}_{\parallel} = (j_x, j_y)$  [Fig. 4(c)],

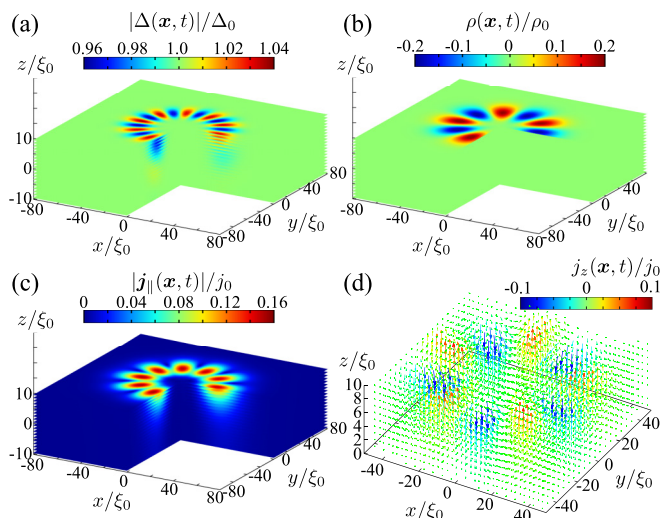


FIG. 4. Snapshots of (a)  $|\Delta(x, t)|$ , (b)  $\rho(x, t)$ , (c)  $|j_{\parallel}(x, t)|$ , and (d)  $\mathbf{j}(x, t)$  at  $t = 51t_{\Delta}$  after the irradiation of the pulsed vortex beam with  $(m, s) = (4, 1)$  and  $\Omega = 1.025\Delta_0$ . In all data, we set  $\kappa_{GL} = 10$ .

after the irradiation of the vortex beam with  $(m, s) = (4, 1)$ . Here, we set  $\Omega = 1.025\Delta_0$  and  $w_0 = 20\xi_0$ . Figure 4(d) is the vectorial plot of  $(j_x, j_y, j_z)$ . In a similar manner to the results observed in a two-dimensional film, the vortex beam induces spiral waves in both the condensate amplitude [Fig. 4(a)] and the phase excitation [Fig. 4(b)], which reflect twice the total angular momentum  $2J$  and the total angular momentum  $J$ , respectively. The amplitude oscillation penetrates the skin depth within  $\lambda$ , while alternative positive and negative charge distributions accumulate on the surface as  $\rho(x, t) \sim A \sin(J\theta - \Omega t)\delta(z - d/2)$ . Such charge distribution creates a three-dimensional flow of the supercurrent density, depicted in Figs. 4(c) and 4(d). Two-dimensional simulations can accurately represent the nonlinear Higgs excitation and THG induced by vortex beams. These characteristics remain consistent as long as the thickness is much shorter than the laser wavelength.

*Concluding remarks.* In this Letter, we have investigated the nonlinear optical responses of superconductors to vortex

beams and examined the possibility of utilizing OAM as an additional degree of freedom. We have demonstrated that vortex beams with nonzero OAM induce the spiral-shaped oscillations in both the condensate and charge density. The phase modes linearly driven by vortex beams facilitate the imprinting of the spiral-shaped wavefront and the transfer of OAM to the condensate. We have also found that increasing the OAM of light amplifies the THG intensity. In Ref. [42], we have further discussed how light and material parameters impact on our key findings. Here, we have identified optimal values for the Ginzburg-Landau parameter and the beam waist to maximize nonlinear Higgs excitation and THG intensity.

We have used the effective action which only takes into account the diamagnetic Higgs response, without considering the contribution of Bogoliubov quasiparticles. For Gaussian beams, however, it has been unveiled that quasiparticle pair excitations play a crucial role in the THG [53,54]. In addition, the third-order paramagnetic current responses [55,56] may also come into play for vortex beams with nonzero OAM even in clean superconductors. Further research is needed to calculate the THG from the gauge-invariant microscopic theory [57–59], including both quasiparticles and the Higgs mode via paramagnetic and diamagnetic channels, beyond Eq. (2).

As we mentioned in the Introduction, applications of structured light have been gradually extending to condensed matter physics [20–26,60–66]. On top of vortex beams, several types of topological light have been developed [67–69]. The present Letter and these works will further accelerate the marriage of topological light with condensed matter physics.

*Acknowledgments.* We thank N. Tsuji, T. Omatsu, and Y. Kawaguchi for useful discussions. This work was supported by a Grant-in-Aid for Scientific Research on Innovative Areas “Quantum Liquid Crystals” (Grants No. JP19H05825 and No. JP22H04480) and “Evolution of Chiral Materials Science using Helical Light Fields” (Grants No. JP22H05131 and No. JP23H04576) from JSPS of Japan, and JSPS KAKENHI (Grants No. JP20K03860, No. JP20H01857, No. JP20H01830, No. JP20H01849, No. JP21H01039, and No. JP22H01221).

- [1] L. Allen, M. W. Beijersbergen, R. J. C. Spreeuw, and J. P. Woerdman, Orbital angular momentum of light and the transformation of Laguerre-Gaussian laser modes, *Phys. Rev. A* **45**, 8185 (1992).
- [2] S. Franke-Arnold, Optical angular momentum and atoms, *Philos. Trans. R. Soc. A* **375**, 20150435 (2017).
- [3] Y. Shen, X. Wang, Z. Xie, C. Min, X. Fu, Q. Liu, M. Gong, and X. Yuan, Optical vortices 30 years on: OAM manipulation from topological charge to multiple singularities, *Light: Sci. Appl.* **8**, 90 (2019).
- [4] H. He, M. E. J. Friese, N. R. Heckenberg, and H. Rubinsztein-Dunlop, Direct observation of transfer of angular momentum to absorptive particles from a laser beam with a phase singularity, *Phys. Rev. Lett.* **75**, 826 (1995).
- [5] T. Kuga, Y. Torii, N. Shiokawa, T. Hirano, Y. Shimizu, and H. Sasada, Novel optical trap of atoms with a doughnut beam, *Phys. Rev. Lett.* **78**, 4713 (1997).
- [6] A. T. O’Neil, I. MacVicar, L. Allen, and M. J. Padgett, Intrinsic and extrinsic nature of the orbital angular momentum of a light beam, *Phys. Rev. Lett.* **88**, 053601 (2002).
- [7] M. P. MacDonald, L. Paterson, K. Volke-Sepulveda, J. Arlt, W. Sibbett, and K. Dholakia, Creation and manipulation of three-dimensional optically trapped structures, *Science* **296**, 1101 (2002).
- [8] J. E. Curtis and D. G. Grier, Structure of Optical Vortices, *Phys. Rev. Lett.* **90**, 133901 (2003).
- [9] K. Dholakia and T. Čížmár, Shaping the future of manipulation, *Nat. Photonics* **5**, 335 (2011).

- [10] A. Mair, A. Vaziri, G. Weihs, and A. Zeilinger, Entanglement of the orbital angular momentum states of photons, *Nature (London)* **412**, 313 (2001).
- [11] J. Wang, J.-Y. Yang, I. M. Fazal, N. Ahmed, Y. Yan, H. Huang, Y. Ren, Y. Yue, S. Dolinar, M. Tur, and A. E. Willner, Terabit free-space data transmission employing orbital angular momentum multiplexing, *Nat. Photonics* **6**, 488 (2012).
- [12] N. Bozinovic, Y. Yue, Y. Ren, M. Tur, P. Kristensen, H. Huang, A. E. Willner, and S. Ramachandran, Terabit-scale orbital angular momentum mode division multiplexing in fibers, *Science* **340**, 1545 (2013).
- [13] T. Omatsu, K. Chujo, K. Miyamoto, M. Okida, K. Nakamura, N. Aoki, and R. Morita, Metal microneedle fabrication using twisted light with spin, *Opt. Express* **18**, 17967 (2010).
- [14] K. Toyoda, K. Miyamoto, N. Aoki, R. Morita, and T. Omatsu, Using optical vortex to control the chirality of twisted metal nanostructures, *Nano Lett.* **12**, 3645 (2012).
- [15] K. Toyoda, F. Takahashi, S. Takizawa, Y. Tokizane, K. Miyamoto, R. Morita, and T. Omatsu, Transfer of light helicity to nanostructures, *Phys. Rev. Lett.* **110**, 143603 (2013).
- [16] M. R. Dennis, R. P. King, B. Jack, K. O'Holleran, and M. J. Padgett, Isolated optical vortex knots, *Nat. Phys.* **6**, 118 (2010).
- [17] M. Harwit, Photon orbital angular momentum in astrophysics, *Astrophys. J.* **597**, 1266 (2003).
- [18] K. Miyamoto, K. Suzuki, T. Akiba, and T. Omatsu, Direct observation of the topological charge of a terahertz vortex beam generated by a Tsurupica spiral phase plate, *Appl. Phys. Lett.* **104**, 261104 (2014).
- [19] T. Arikawa, T. Hiraoka, S. Morimoto, F. Blanchard, S. Tani, T. Tanaka, K. Sakai, H. Kitajima, K. Sasaki, and K. Tanaka, Transfer of orbital angular momentum of light to plasmonic excitations in metamaterials, *Sci. Adv.* **6**, eaay1977 (2020).
- [20] A. A. Sirenko, P. Marsik, C. Bernhard, T. N. Stanislavchuk, V. Kiryukhin, and S.-W. Cheong, Terahertz vortex beam as a spectroscopic probe of magnetic excitations, *Phys. Rev. Lett.* **122**, 237401 (2019).
- [21] H. Wang, Q. Song, Y. Cai, Q. Lin, X. Lu, H. Shangguan, Y. Ai, and S. Xu, Recent advances in generation of terahertz vortex beams and their applications, *Chin. Phys. B* **29**, 097404 (2020).
- [22] A. A. Sirenko, P. Marsik, L. Bugnon, M. Soulier, C. Bernhard, T. N. Stanislavchuk, X. Xu, and S.-W. Cheong, Total angular momentum dichroism of the terahertz vortex beams at the antiferromagnetic resonances, *Phys. Rev. Lett.* **126**, 157401 (2021).
- [23] J. Ishihara, T. Mori, T. Suzuki, S. Sato, K. Morita, M. Kohda, Y. Ohno, and K. Miyajima, Imprinting spatial helicity structure of vector vortex beam on spin texture in semiconductors, *Phys. Rev. Lett.* **130**, 126701 (2023).
- [24] M. A. Yavorsky, M. A. Kozhaev, A. Y. Fedorov, D. V. Vikulin, E. V. Barshak, V. N. Berzhansky, S. D. Lyashko, P. O. Kapralov, and V. I. Belotelov, Topological faraday effect for optical vortices in magnetic films, *Phys. Rev. Lett.* **130**, 166901 (2023).
- [25] H. Fujita and M. Sato, Encoding orbital angular momentum of light in magnets, *Phys. Rev. B* **96**, 060407(R) (2017).
- [26] H. Fujita and M. Sato, Ultrafast generation of skyrmionic defects with vortex beams: Printing laser profiles on magnets, *Phys. Rev. B* **95**, 054421 (2017).
- [27] D. G. Hall, Vector-beam solutions of Maxwell's wave equation, *Opt. Lett.* **21**, 9 (1996).
- [28] R. Matsunaga, Y. I. Hamada, K. Makise, Y. Uzawa, H. Terai, Z. Wang, and R. Shimano, Higgs amplitude mode in the BCS superconductors  $\text{Nb}_{1-x}\text{Ti}_x\text{N}$  induced by terahertz pulse excitation, *Phys. Rev. Lett.* **111**, 057002 (2013).
- [29] R. Matsunaga, N. Tsuji, H. Fujita, A. Sugioka, K. Makise, Y. Uzawa, H. Terai, Z. Wang, H. Aoki, and R. Shimano, Light-induced collective pseudospin precession resonating with Higgs mode in a superconductor, *Science* **345**, 1145 (2014).
- [30] D. Sherman, U. S. Pracht, B. Gorshunov, S. Poran, J. Jesudasan, M. Chand, P. Raychaudhuri, M. Swanson, N. Trivedi, A. Auerbach, M. Scheffler, A. Frydman, and M. Dressel, The Higgs mode in disordered superconductors close to a quantum phase transition, *Nat. Phys.* **11**, 188 (2015).
- [31] K. Katsumi, N. Tsuji, Y. I. Hamada, R. Matsunaga, J. Schneeloch, R. D. Zhong, G. D. Gu, H. Aoki, Y. Gallais, and R. Shimano, Higgs mode in the  $d$ -wave superconductor  $\text{Bi}_2\text{Sr}_2\text{CaCu}_2\text{O}_{8+x}$  driven by an intense terahertz pulse, *Phys. Rev. Lett.* **120**, 117001 (2018).
- [32] S. Nakamura, Y. Iida, Y. Murotani, R. Matsunaga, H. Terai, and R. Shimano, Infrared activation of the higgs mode by supercurrent injection in superconducting NbN, *Phys. Rev. Lett.* **122**, 257001 (2019).
- [33] S. Nakamura, K. Katsumi, H. Terai, and R. Shimano, Nonreciprocal terahertz second-harmonic generation in superconducting NbN under supercurrent injection, *Phys. Rev. Lett.* **125**, 097004 (2020).
- [34] K. Katsumi, Z. Z. Li, H. Raffy, Y. Gallais, and R. Shimano, Superconducting fluctuations probed by the Higgs mode in  $\text{Bi}_2\text{Sr}_2\text{CaCu}_2\text{O}_{8+x}$  thin films, *Phys. Rev. B* **102**, 054510 (2020).
- [35] R. Shimano and N. Tsuji, Higgs mode in superconductors, *Annu. Rev. Condens. Matter Phys.* **11**, 103 (2020).
- [36] H. Chu, M.-J. Kim, K. Katsumi, S. Kovalev, R. D. Dawson, L. Schwarz, N. Yoshikawa, G. Kim, D. Putzky, Z. Z. Li *et al.*, Phase-resolved Higgs response in superconducting cuprates, *Nat. Commun.* **11**, 1793 (2020).
- [37] C. Vaswani, J. H. Kang, M. Mootz, L. Luo, X. Yang, D. Cheng, C. Huang, R. H. J. Kim, Z. Liu, Y. G. Collantes, E. E. Hellstrom, I. E. Perakis, C. B. Eom, and J. Wang, Light quantum control of persisting Higgs modes in iron-based superconductors, *Nat. Commun.* **12**, 258 (2021).
- [38] R. Grasset, K. Katsumi, P. Massat, H.-H. Wen, X.-H. Chen, Y. Gallais, and R. Shimano, Terahertz pulse-driven collective mode in the nematic superconducting state of  $\text{Ba}_{1-x}\text{K}_x\text{Fe}_2\text{As}_2$ , *npj Quantum Mater.* **7**, 4 (2022).
- [39] H. T. C. Stoof, Time-dependent Ginzburg-Landau theory for a weak-coupling superconductor, *Phys. Rev. B* **47**, 7979 (1993).
- [40] D. Pekker and C. M. Varma, Amplitude/Higgs modes in condensed matter physics, *Annu. Rev. Condens. Matter Phys.* **6**, 269 (2015).
- [41] A. R. Hammer and A. B. Vorontsov, Bound collective modes in nonuniform superconductors, *Phys. Rev. B* **93**, 014503 (2016).
- [42] See Supplemental Material at <http://link.aps.org/supplemental/10.1103/PhysRevResearch.5.L042004> for details of the effective action, the methods of numerical simulations, the parameter dependences of the numerical results, and GIF files demonstrating the dynamics of the superconductor.
- [43] M. Donaire, T. W. B. Kibble, and A. Rajantie, Spontaneous vortex formation on a superconducting film, *New J. Phys.* **9**, 148 (2007).

- [44] K. Moriarty, E. Myers, and C. Rebbi, Dynamical interactions of cosmic strings and flux vortices in superconductors, *Phys. Lett. B* **207**, 411 (1988).
- [45] R. Kato, Y. Enomoto, and S. Maekawa, Computer simulations of dynamics of flux lines in type-II superconductors, *Phys. Rev. B* **44**, 6916 (1991).
- [46] Q. Du, Global existence and uniqueness of solutions of the time-dependent Ginzburg-Landau model for superconductivity, *Appl. Anal.* **53**, 1 (1994).
- [47] W. D. Gropp, H. G. Kaper, G. K. Leaf, D. M. Levine, M. Palumbo, and V. M. Vinokur, Numerical simulation of vortex dynamics in type-II superconductors, *J. Comput. Phys.* **123**, 254 (1996).
- [48] J. B. Kogut, An introduction to lattice gauge theory and spin systems, *Rev. Mod. Phys.* **51**, 659 (1979).
- [49] R. Meservy and B. B. Schwartz, Equilibrium properties: Comparison of experimental results with predictions of the BCS theory, in *Superconductivity*, edited by R. D. Parks (Dekker, New York, 1969), p. 117.
- [50] S. P. Chockalingam, M. Chand, J. Jesudasan, V. Tripathi, and P. Raychaudhuri, Superconducting properties and Hall effect of epitaxial NbN thin films, *Phys. Rev. B* **77**, 214503 (2008).
- [51] Y. Toda, H. Mochizuki, S. Tsuchiya, T. Kurosawa, M. Oda, T. Mertelj, and D. Mihailovic, Nonequilibrium quasiparticle dynamics in Bi-based superconductors measured by modulation photoexcitation spectroscopy, *J. Supercond. Novel Magn.* **31**, 753 (2018).
- [52] Y. Toda, S. Tsuchiya, K. Yamane, R. Morita, M. Oda, T. Kurosawa, T. Mertelj, and D. Mihailovic, Optical vortex induced spatio-temporally modulated superconductivity in a high- $T_c$  cuprate, *Opt. Express* **31**, 17537 (2023).
- [53] T. Cea, C. Castellani, and L. Benfatto, Nonlinear optical effects and third-harmonic generation in superconductors: Cooper pairs versus Higgs mode contribution, *Phys. Rev. B* **93**, 180507(R) (2016).
- [54] N. Tsuji and H. Aoki, Theory of Anderson pseudospin resonance with Higgs mode in superconductors, *Phys. Rev. B* **92**, 064508 (2015).
- [55] T. Jujo, Quasiclassical theory on third-harmonic generation in conventional superconductors with paramagnetic impurities, *J. Phys. Soc. Jpn.* **87**, 024704 (2018).
- [56] M. Silaev, Nonlinear electromagnetic response and Higgs-mode excitation in BCS superconductors with impurities, *Phys. Rev. B* **99**, 224511 (2019).
- [57] R. M. Lutchyn, P. Nagornykh, and V. M. Yakovenko, Gauge-invariant electromagnetic response of a chiral  $p_x + ip_y$  superconductor, *Phys. Rev. B* **77**, 144516 (2008).
- [58] H. Rostami, M. I. Katsnelson, G. Vignale, and M. Polini, Gauge invariance and Ward identities in nonlinear response theory, *Ann. Phys.* **431**, 168523 (2021).
- [59] A. A. Radkevich and A. G. Semenov, Nonlinear microwave response of clean superconducting films, *Phys. Rev. B* **106**, 094505 (2022).
- [60] M. F. Andersen, C. Ryu, P. Cladé, V. Natarajan, A. Vaziri, K. Helmerson, and W. D. Phillips, Quantized rotation of atoms from photons with orbital angular momentum, *Phys. Rev. Lett.* **97**, 170406 (2006).
- [61] T. P. Simula, N. Nygaard, S. X. Hu, L. A. Collins, B. I. Schneider, and K. Mølmer, Angular momentum exchange between coherent light and matter fields, *Phys. Rev. A* **77**, 015401 (2008).
- [62] H.-R. Chen, K.-Y. Lin, P.-K. Chen, N.-C. Chiu, J.-B. Wang, C.-A. Chen, P. Huang, S.-K. Yip, Y. Kawaguchi, and Y.-J. Lin, Spin-orbital-angular-momentum coupled Bose-Einstein condensates, *Phys. Rev. Lett.* **121**, 113204 (2018).
- [63] H. Fujita and M. Sato, Nonequilibrium magnetic oscillation with cylindrical vector beams, *Sci. Rep.* **8**, 15738 (2018).
- [64] H. Fujita, Y. Tada, and M. Sato, Accessing electromagnetic properties of matter with cylindrical vector beams, *New J. Phys.* **21**, 073010 (2019).
- [65] M. El Ketara, H. Kobayashi, and E. Brasselet, Sensitive vectorial optomechanical footprint of light in soft condensed matter, *Nat. Photonics* **15**, 121 (2021).
- [66] A. A. Gunyaga, M. V. Durnev, and S. A. Tarasenko, Photocurrents induced by structured light, *Phys. Rev. B* **108**, 115402 (2023).
- [67] Q. Zhan, Cylindrical vector beams: From mathematical concepts to applications, *Adv. Opt. Photonics* **1**, 1 (2009).
- [68] Y. Wu, Q. Wu, F. Sun, C. Cheng, S. Meng, and J. Zhao, Emergence of electron coherence and two-color all-optical switching in MoS<sub>2</sub> based on spatial self-phase modulation, *Proc. Natl. Acad. Sci. USA* **112**, 11800 (2015).
- [69] C. He, Y. Shen, and A. Forbes, Towards higher-dimensional structured light, *Light: Sci. Appl.* **11**, 205 (2022).